Few-Mode Metal-Free Perovskite Optical Fibre with Second-Order Optical Nonlinearity

H. C. L. Tsui,[1] D. Sirbu,[1] N. Alsaif,[1] N. Hill,[1] Graham Tizzard,[2] Pablo Docampo,[3] and N. Healy[1]

[1)] *Emerging Technologies and Materials Group, School of Mathematics, Statistics and Physics, Newcastle University, Newcastle, NE1 7RU, UK*

[2)] *School of Chemistry, University of Southampton, Southampton, SO17 1BJ, UK*

[3)] *School of Chemistry, University of Glasgow, Glasgow, G12 8QQ, UK*

(*Electronic mail: noel.healy@newcastle.ac.uk)

(Dated: 30 January 2024)

Semiconductor core optical fibres are highly desirable for fibre-based photonic and optoelectronic applications as they can combine strong optical nonlinearities, tight light confinement, wide transmission bands, and electronic functionality within a single platform. Perovskites have emerged as particularly exciting materials for semiconductor photonics as they have strong optical nonlinearities and tunable optoelectronic band gaps. However, lead-based perovskites contain toxic elements and are therefore not environmentally friendly. Furthermore, in fibre form, their core-size is prohibitively large, making them unsuitable for nonlinear optics and applications that require single-mode guidance, such as telecommunications. Here, we report a metal-free perovskite core optical fibre where lead has been substituted for an ammonium cation in the perovskite structure. The core material has a wide band gap greater than 5 eV, a high laser damage threshold, and a core diameter that can be produced as small as 5 µm. At this core size the fibre supports just six modes and the fundamental mode can readily be excited and isolated. Moreover, the metal-free perovskite has a second-order susceptibility that is absent in the archetypal lead-based perovskites and many other semiconductor core materials, such as silicon and germanium. The second-order susceptibility is important for many nonlinear optics applications such as second-harmonic generation and quantum optics.

I. INTRODUCTION

Semiconductor core optical fibres are a relatively nascent technology that provides excellent nonlinear and electro-optical properties in a waveguiding architecture. These properties have been leveraged in a wide range of devices that include photovoltaic cells, in-fibre detectors, all-optical modulators and supercontinuum generators[1–8]. To date, most of the demonstrators have used simple unary semiconductor core materials such as silicon and germanium, but, more recently there has been increasing interest in more complex binary and ternary semiconductor systems[9–14]. These have extended the functionality of the platform, for example, providing direct band gap materials for efficient light sources or photodetectors[10,15–17]. While efforts have been made to incorporate perovskite nanocrystals in optical fibre-type application[18–20], one exciting development in the field is the demonstration of semiconductor optical fibres with organometallic halide perovskite cores[21,22]. Perovskites have superlative electronic, optical, and nonlinear optical properties and their integration with the fibre platform represents a step change for functional optical fibre technologies. The highly tunable nature of the material means that its properties can be tailored for specific target applications. For example, the high third-order nonlinearity, efficient light emission, and selectable band gap could, in the future, be harnessed for applications that generate, convert, guide and detect light[23–33].

Aside from the obvious toxicity issues associated with the lead content, there are other shortcomings in the current state-of-the-art of perovskite optical fibres that precludes their use for the above mentioned applications. For example, nonlinear optics requires high energy densities and for a fibre device, this means a small core or, more specifically, tight confinement of the propagating mode. The current method of producing perovskite optical fibres uses a solution-based, space-confined, inverse temperature crystallization approach and owing to issues with solvent transport the smallest core diameter of glass-clad perovskite optical fibres achievable are upwards of 100 µm[22]. By using PTFE in place of the glass cladding, modified wetting kinetics allow for further reduction of the core diameter down to 50 µm. At these core sizes, the optical fibres are highly multi-moded and not amenable to nonlinear optics applications. Furthermore, the archetypal perovskites are designed to absorb visible light and are therefore not attractive for waveguiding in the visible region of the spectrum.

In this work, we explore an iodide-based metal-free perovskite[34,35] as the core material for an optical fibre. Here, we substitute the metal Pb^{2+} centre in the hybrid perovskite archetypal structure for an NH_4^+ cation and use methyl-1,4-diazoniumbicyclo[2.2.2]octane ($MDABCO^{2+}$) as the spacer cation, yielding Methyl-DABCO Ammonium Iodide (MDNI)[36].

This immediately addresses the problem of toxicity but also presents other exciting opportunities. We have previously shown that MDNI maintains the strong third-order nonlinearity associated with the perovskite crystal structure and it has a wide band gap of greater than 5 eV, making it a strong candidate for nonlinear optics applications from the near-infrared to the ultra-violet[36]. The incorporation of the polar MDBACO cation into the lattice produces a corner-sharing 3D trigonal R_3 perovskite structure with ammonium halide octahedra, Figure 1a. As shown in Figure 1b, these octahedra are distorted which means that the crystal is not centrosymmetric, making them ferroelectric materials with a permanent dipole at room temperature and therefore a non-zero second-

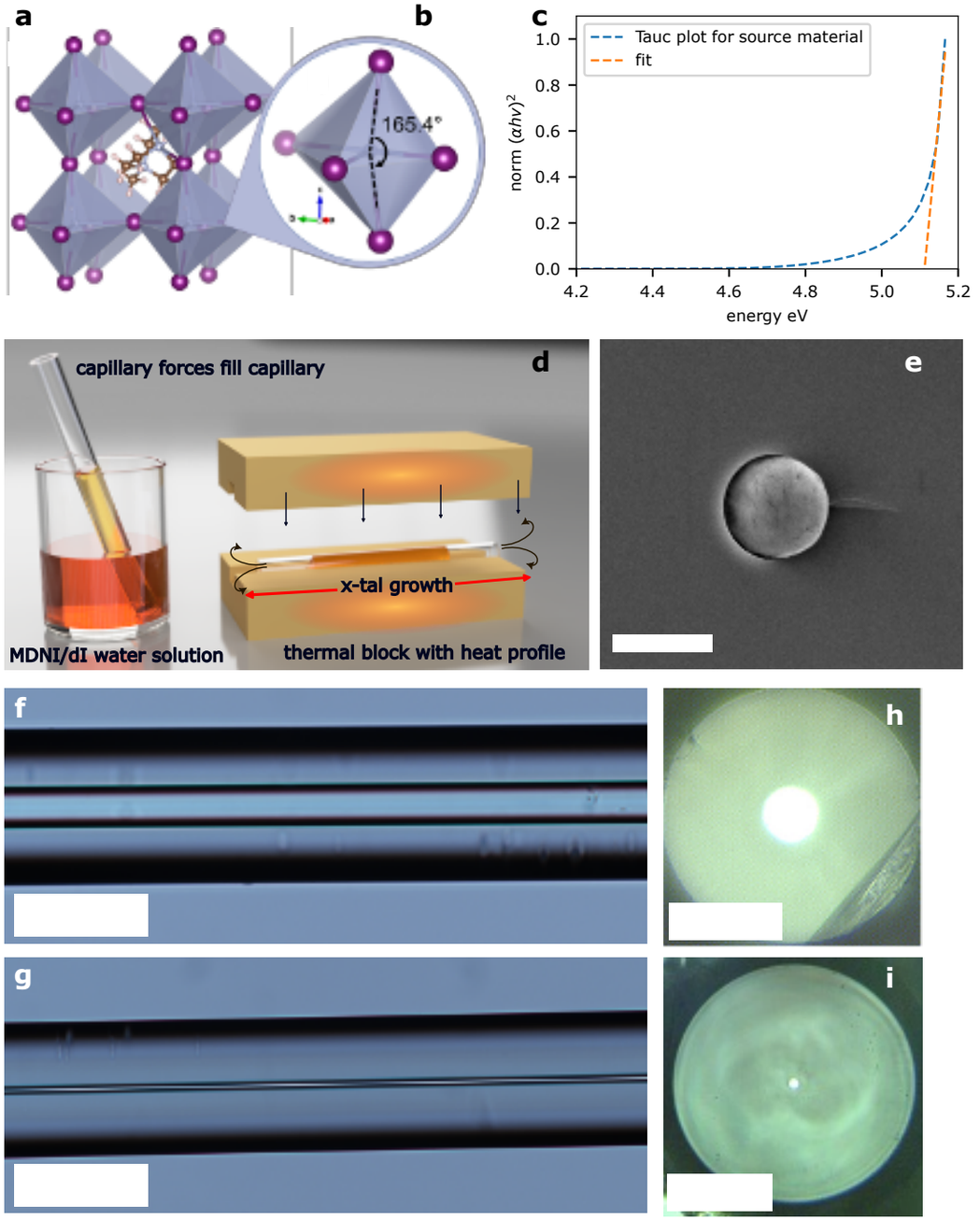

FIG. 1. **a** Side view of the MDNI crystal packing showing the octahedra. **b** Highlight of the distortion of the NH_4I_6 octahedra responsible for the emergence of a non-zero second-order susceptibility. **c** a Tauc plot generated from UV-VIS (Figure S2) measurements of the synthesised MDNI crystal. **d** Schematic of the capillary action method of precursor solution deposition and subsequent crystallisation. **e** Scanning electron microscope image of the cleaved cross-section of a 5 µm MDNI core optical fibre, scale bar 5 µm. **f** Diascopic image of the side of a 25 µm MDNI core optical fibre, scale bar 100 µm. **g** Diascopic image of the side of a 5 µm MDNI core optical fibre, scale bar 100 µm. Diascopic illumination and microscope image of **h** a 25 µm MDNI core optical fibre and **i** a 5 µm MDNI core optical fibre, showing white light confined to each core, scale bars 50 µm.

order nonlinearity, that in this instance, is predicted by density functional theory to be 2 pm V^{-1}; moreover, like the third order nonlinearity, this is highly tuneable by varying the spacer cation[36,37]. In fact, previous studies show that ferroelectricity in these materials is responsible for efficient and polarization-dependent second-harmonic generation (SHG)[38]. These properties and resulting capabilities, i.e., SHG and parametric down-conversion coupled with simple processability and high

laser damage thresholds, make this emerging family of metal-free perovskites extremely attractive for optoelectronic and quantum optics applications.

Here, we present the first demonstration of an optical fibre with a metal-free perovskite (MDNI) core. By adopting a conventional crystallisation process, i.e., controlled cooling, fibres with core sizes of 5 µm can be readily produced within a glass (SiO_2) cladding. The fibre is few-moded and supports just six modes with the fundamental mode tightly confined to the core, thus providing a route to perovskite fibre-based nonlinear optics. We demonstrate this potential by showing second-harmonic generation in the core, which is permitted by the non-centrosymmetric core material; a property that eludes the organometallic halide perovskite family.

II. RESULTS AND DISCUSSIONS

A. Fabrication of metal-free perovskite optical fibres

Large crystals of MDNI were synthesised using the protocol outlined in the Experimental Section and the crystal structure of MDNI was confirmed using *X*-ray diffraction, see Supplementary Materials Figure S2. Figure 1c shows a Tauc plot derived from UV-VIS measurements (Figure S3, Supplementary Materials) confirming the expected wide band gap of the material to be 5.11 eV. The core of the optical fibre is grown from a solution of this source MDNI in deionised water. The silica cladding capillaries can be filled with the solution via capillary action or, for longer lengths, a method of forcing the liquid into the capillary can be used, see Figure 1d. The crystalline core material is grown from the solution by placing it in an oven and slowly cooling the liquid from 95 °C to room temperature, i.e., via standard supersaturation, nucleation and growth, Figure 1d. Here, the concentration is higher at the edge of the capillary tube, as water is slowly evaporated, nucleating the crystal and promoting its slow growth across the tube. This process negates the solvent transport issues associated with the inverse temperature crystallization approach and allows the growth of the core material at orders of magnitude smaller core dimensions without having to substitute or modify the silica cladding capillaries for alternative less optical fibre network-compatible materials. A detailed description of the fibre fabrication is provided in the Experimental Section.

Figure 1e shows an SEM of the cross-section of a cleaved 5 µm core diameter MDNI optical fibre that has been deposited by this approach. It is clear that the core completely and conformally fills the capillary cladding. Figures 1f-g show diascopically illuminated microscope images of longitudinal sections of (f) a 25 µm core diameter MDNI core optical fibre and that of (g) a 5 µm MDNI core diameter optical fibre. The core material is highly transparent owing to the high quality of the crystal and its wide band gap. The deposited structures can have a uniform cross-section for as long as 3 cm which represents an aspect ratio of 3×10^5 for the 5 µm core optical fibre (Figure S1, Supplementary Materials). The end faces of the optical fibres can be readily polished using a standard 'dry' optical fibre polishing procedure. Figure 1h-i are microscope images of the polished (h) 25 µm and (i) 5 µm fibres under diascopic illumination and both clearly show white light being guided by the core. A transmission spectrum from the ultra-violet to the near infrared can be seen in the Supplementary Materials Figure S4.

B. Characterisation of the core material of metal-free perovskite optical fibres

Raman spectroscopy measurements of the 5 µm MDNI fibre were undertaken by focussing a 532 nm laser through the cladding of the fibre onto the core and collecting the scattered light. This spectrum was compared to that of a single crystal of MDNI taken using the same conditions, both are shown in Figure 2a. The low-frequency Raman modes, between $80\,cm^{-1}$ and $400\,cm^{-1}$, can be assigned to the lattice modes and these have a broad weak signal in both the single crystal and the MDNI fibre which can be attributed to dynamic disorder of the organic ions[39]. The $MDABCO^{2+}$ related vibrations between $600\,cm^{-1}$ and $1200\,cm^{-1}$ exhibit strong sharp peaks and the comparison between the single crystal and the core material indicates a high degree of core material crystallinity. Lorentzian fitting of the peak at $696\,cm^{-1}$ for each spectrum, shown in Figure 2b, indicates that the MDNI fibre core and the single crystal sample have very similar full-width at half-maximum, measured to be $3.11\,cm^{-1}$ and $3.1\,cm^{-1}$, respectively. This result shows that the core material of the fibre is highly crystalline. The symmetry of the peak for the fibre core material is further evidence of the high crystallinity, as asymmetry can be caused by a high concentration of crystalline defects.

X-ray diffraction (XRD) was performed on as grown core material that was ground from the cores of the 25 µm MDNI optical fibre and the result was compared to that of a powder created from a single crystal of MDNI, these results are shown in Figure 2c and confirm good phase purity in the MDNI core material. To further investigate the crystalline nature of the core material both MDNI optical fibres were mounted in a Lindemann tube and single crystal XRD experiments were undertaken along the length at predetermined intervals. The spot-size of the *X*-ray beam was 85 µm, thus sampling the entire core diameter of each fibre. Though large single crystals are observed in these measurements, they were randomly orientated and there was no preferential orientation of the crystal within each core, which has been evident in other semiconductor optical fibre crystallisation technologies[40]. The crystal structure was resolved to be trigonal in the R_3 space group with a lattice parameter of $a = 9.7018(2)$ Å, $b = 9.7018(2)$ Å, $c = 13.4526(4)$ Å, $\alpha = 90°$, $\beta = 90°$, and $\gamma = 120°$ consistent with that expected for MDNI[35]. Figure 1d is an image of the resolved crystal structure demonstrating the R_3 space group packing. Supplementary Materials Figure S5 provides views along the *a*, *b*, and *c* axes. Figure 1e shows the Ewald sphere generated via *X*-ray diffraction of a 5 µm MDNI fibre core showing a single crystal across the entire core diameter. The estimated average grain size in the 5 µm core fibre was of the order of 100 µm with the largest length of single crystal

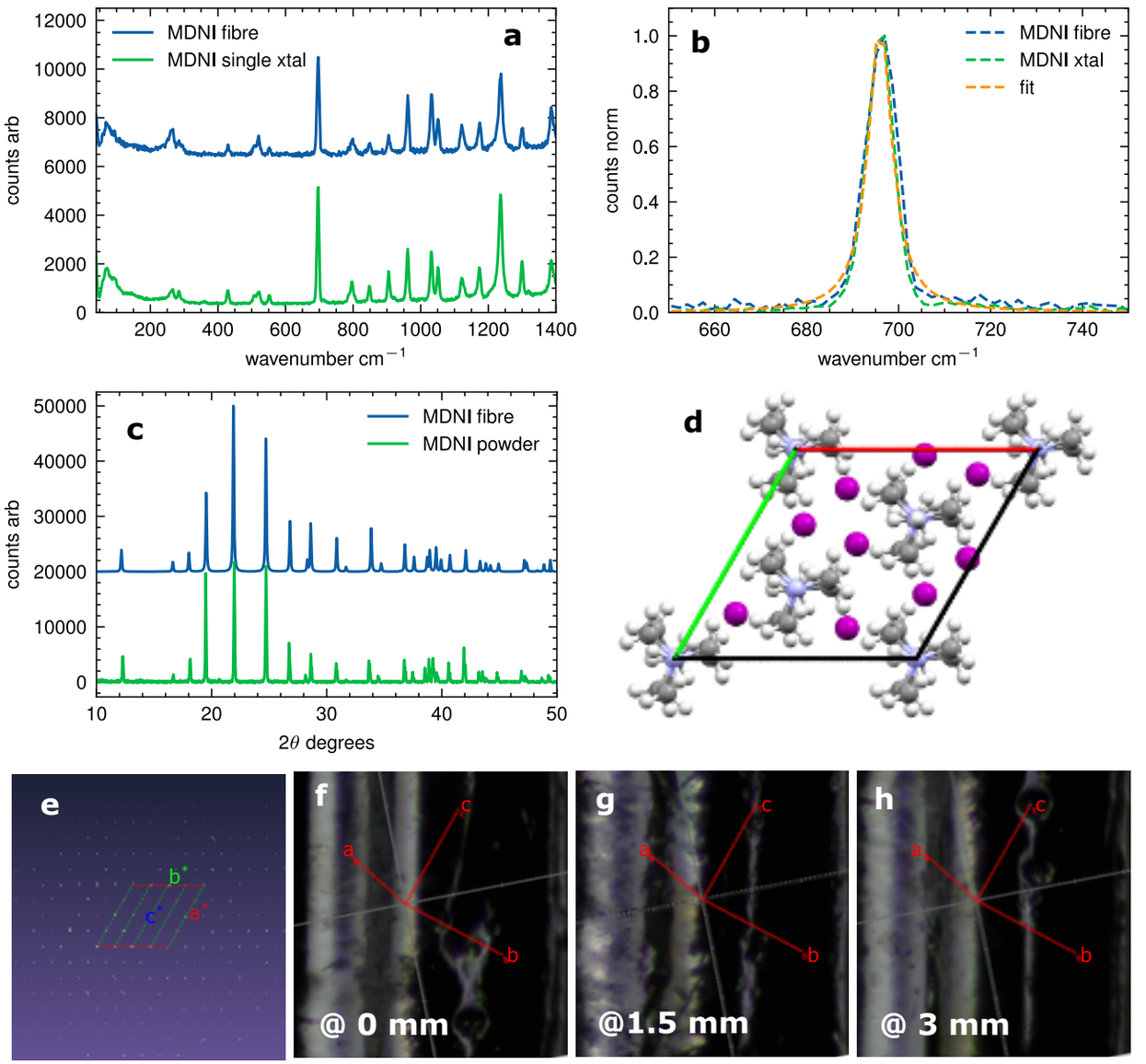

FIG. 2. **a** Raman spectra of the core material (blue) and a single crystal of MDNI (green). **b** Normalised peak of the Raman spectra at 696 cm^{-1} and the Lorentzian fit for the core material. **c** *X*-ray diffractograms of the MDNI core material (blue) and a powdered MDNI sample (green). **d** Single crystal XRD resolved crystal structure of MDNI core material showing the packing of the crystal. Pink = I, white = H, grey = C, light purple = N. **e** Orthogonal projection of the Ewald sphere along the crystallographic reciprocal *c*-axis of a single crystal measured in the 5 µm core MDNI fibre. Image of 25 µm core fibre hosted in a mounting capillary with an overlay of the measured crystallographic direct axes overlaid at three different positions; **f** 0 mm, **g** 1.5 mm, **h** 3 mm.

being in the order of 1 mm (Figure S7, Supplementary Materials). Figure 1f-h show the orientation of the crystal projected onto the 25 µm core fibre as mounted and at the position of measurement. These projections show that there is a dominant crystal along the entire 3 mm sampled region with some crystal twinning observed (Figure S7, Supplementary Materials). The reduction in crystal grain size as related to reduced core sizes led us to using the 5 µm core fibre as the smallest for our optical measurements as this provided a good balance between material quality and transmitted energy density for nonlinear applications.

C. Perovskite optical fibre characterisation

Figures 3a-b show light transmitted through a 1 cm length of 5 µm MDNI core optical fibre at 633 nm and 1550 nm respectively, demonstrating the high bandwidth capability of the

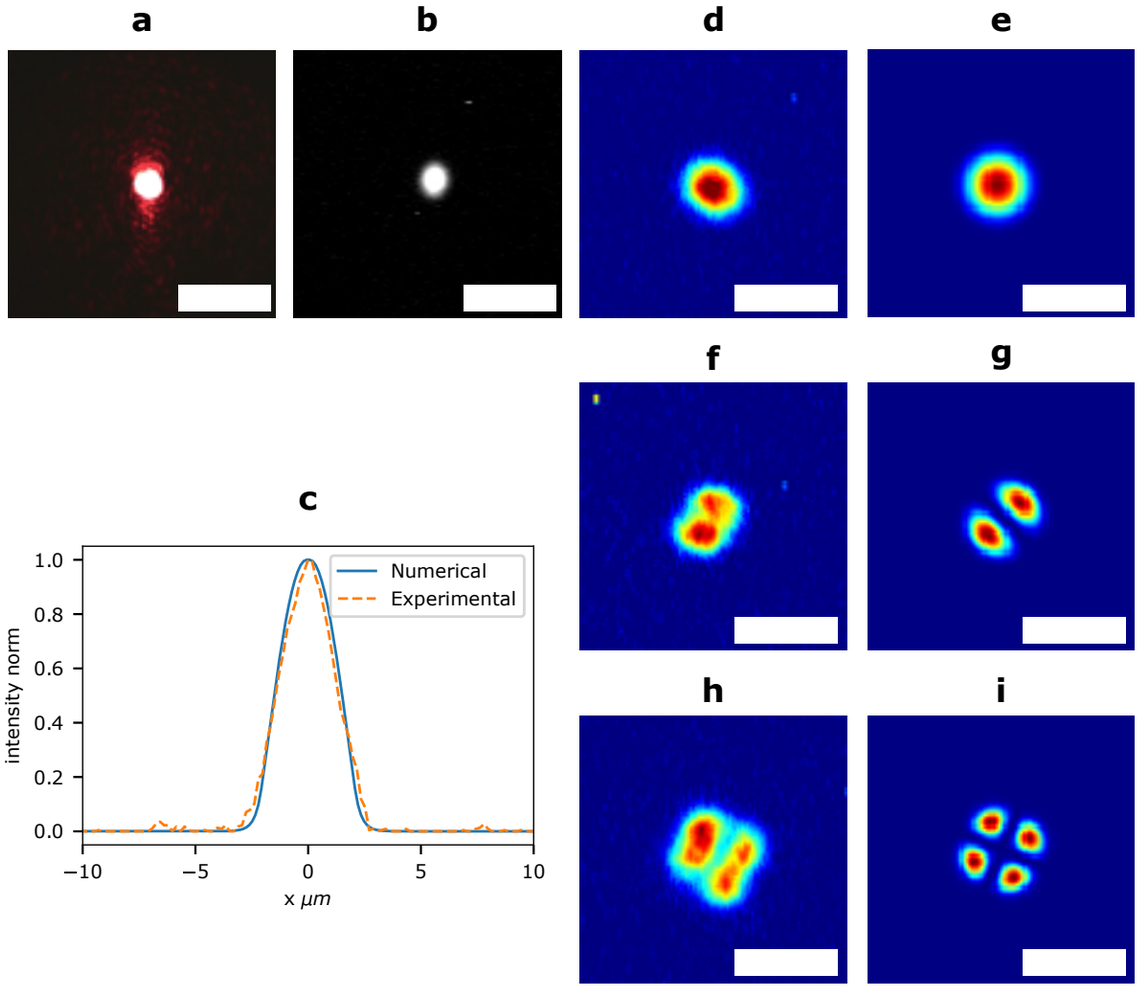

FIG. 3. **a** Transmission of light with a wavelength of 633 nm through a 5 µm MDNI core optical fibre, scale bar 15 µm. **b** Transmission of light with a wavelength of 1550 nm through a 5 µm MDNI core optical fibre, scale bar 15 µm. **c** Measured (orange dashed) and simulated (blue) mode profile from the 5 µm MDNI core optical fibre transmitting 1550 nm light in the fundamental mode. Intensity profile of 1550 nm light transmitted in the 5 µm MDNI core optical fibre via the LP01 mode **d** (experimental) and **e** (numerical simulation), the LP11 mode **f** (experimental) and **g** (numerical simulation), and the LP21 mode **h** (measured) and **i** (numerical simulation), scale bars 10 µm.

optical fibre. The wide band gap of MDNI would, in principle, guide light with low loss down to 250 nm. A detailed optical characterisation of the 5 µm MDNI core optical fibre was undertaken at the important telecommunications wavelength of 1550 nm. The optical transmission loss of the fibre was measured using the standard cut-back approach and a loss of 3 dB cm^{-1} was determined which is commensurate with state-of-the-art semiconductor optical fibres. For this experiment, 1 mm sections were removed from a 1 cm length of the fibre. At these short lengths, it is important that stray cladding light does not lead to underestimation of the losses, however, as is shown in Figures 3b-c all of the light is very tightly confined to the small core. We attribute the losses in the fibre to defects and grain boundaries in the crystalline core. A clear route to reducing these losses would be to increase the core's crystallinity via further optimisation of the deposition process. The core material of the fibre has a refractive index of $n_1 = 1.58$ at 1550 nm and the V-number given by $V = \frac{2\pi a}{\lambda}\sqrt{n_1^2 - n_2^2}$ is 6.48, where λ is the operating wavelength, a is the core radius and the cladding refractive index is $n_2 = 1.444$. As $\Delta n << 1$ the low order modes can be considered as LP modes and at, $V = 6.48$, the fibre can support six LP modes.

An infrared camera was used to image the near-field modes that could be excited in the fibre. Figures 3d,f,h show the experimentally imaged LP01, LP11, and LP21 modes which show good agreement with the same modes produced by finite element modelling simulations of the same fibre, shown in Figure 3e,g,i (see Supplementary Materials Figure S8 for simulation of all modes supported by the fibre). Importantly, the coupling is preferentially obtained into the fundamental LP01 mode, with the higher order modes only being isolated when the input beam is launched off-axis to the core. The

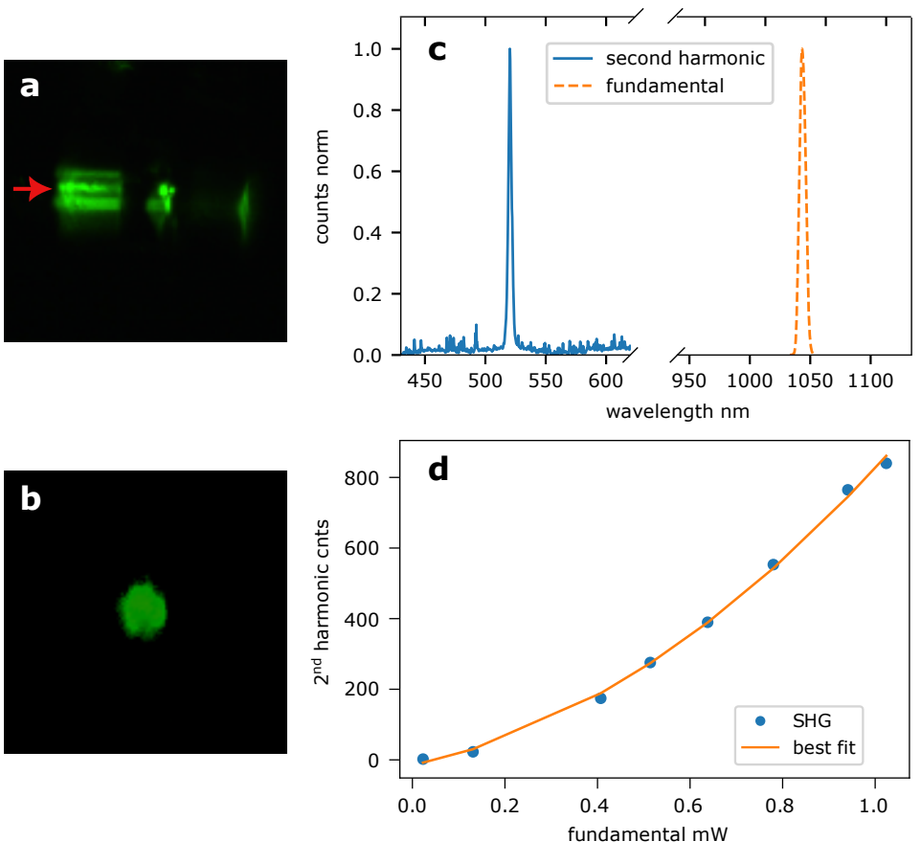

FIG. 4. **a** Image of second-harmonic generated light scattered as it propagates through the 5 µm MDNI core optical fibre (black regions is where the fibre is held to v-groove). **b** The second-harmonic light that is confined to the core as it exits the output of the optical fibre. **c** Spectrum of the fundamental pump beam (orange) and the transmitted second-harmonic (blue) through a 5 µm MDNI core optical fibre. **d** The dependence of the second-harmonic generation on the fundamental pump power showing a parabolic relationship.

slight asymmetries seen in the mode profiles of the higher order modes are most likely due to modest mixing between the allowed modes. Concerning the fundamental mode, the full-width at half-maximum (FWHM) value at the $1/e^2$ power level is 3.8 µm which matches well with the 3.7 µm predicted by our model, see Figure 3c, and with the 3.74 µm predicted by the Marcuse equation at the fibre's V-number[41]. The effective mode area of fundamental mode for this fibre is 11 µm^2, which is two orders of magnitude smaller that the state-of-the-art polymer-clad perovskite fibres and more than three orders of magnitude smaller than the glass-clad organometallic halide perovskite equivalent. Moreover, being able to excite and isolate the fundamental mode is of particular value for nonlinear optics applications.

D. Second-harmonic generation

To demonstrate the fibre for nonlinear optics applications we exploit the lack of centrosymetry in the core material's crystal structure that gives rise to a second-order susceptibility. A 5 µm diameter core MDNI fibre is set-up in a transmission measurement configuration similar to that used to determine the linear optical propagation characteristics. A laser with a wavelength of $\lambda_p = 1040$ nm, a pulse duration of 300 fs, and a repetition rate of 1 kHz was coupled into the optical fibre's fundamental mode. The peak power of the pump laser was increased to elicit a nonlinear response of the transmitted light-matter interaction. As the second-harmonic associated with the pump is expected to be at a wavelength 520 nm, i.e., is green, it was relatively straightforward to detect, filter, and image using a CCD camera, as illustrated in Figure 4a, which shows the second-harmonic response along the length of the fibre. An image of the second-harmonic light that has been transmitted through the fibre is shown in Figure 4b and in this instance, the second-harmonic output has coupled to higher-order modes in the fibre. At this wavelength, the fibre has a $V = 20$ and supports approximately 200 modes, this offers the prospect of modal phase-matching of the second-harmonic to the pump, but we note here, no attempt of phase matching was undertaken in this work. The transmitted light was coupled into a spectrometer and the spectrum of the pump and second-harmonic are shown in Figure 4c. As expected the central wavelength of the second-harmonic is at 520 nm, half that of the fundamental pump. It is also clear that second-harmonic narrowing is present and that the FWHM of the

second-harmonic is $0.42\times$ that of the fundamental, this is identical to the narrowing measured for KDP and close to the theoretically predicted $1/2\sqrt{2}$[42]. Figure 4d plots the power dependence of the second-harmonic signal, exhibiting a clear quadratic relation, which further confirms that the visible signal is produced by second-harmonic originating from the core material's second-order nonlinearity.

III. CONCLUSION

We have demonstrated the first optical fibre employing a metal-free perovskite as the core material. We demonstrate that the MDNI crystalline core can be grown via simple cooling of a supersaturated solution, opening up a route for fibre fabrication with the wide array of metal-free perovskites that are being developed. The fibre that we have presented in this work is a few-mode fibre that allows robust, single-mode operation while maintaining tight light confinement in the active core material. This is an important step for perovskite optical fibres as single-mode operation is important for many applications, including those for telecommunications. Unlike the archetypal organometallic perovskites that were designed for solar applications, the metal-free MDNI core material has a wide band gap and permits the guidance of visible light. Furthermore, MDNI, like many metal-free perovskites lacks a centrosymmetric crystal structure which means that it can be used for many important second-order nonlinear optical applications, for example, electrooptic modulation, harmonic generation, and parametric down-conversion[43]. Owing to the versatility of the perovskite structure, these materials can be developed to enhance their nonlinear properties and being able to produce fibre waveguiding devices for a wide-ranging set of applications, for example, all-optical signal processing, supercontinuum generation, frequency comb generation, and quantum optics[44].

IV. EXPERIMENTAL

A. MDNI synthesis

1,4-Diazabicyclo[2.2.2]octane (DABCO), NH_4I and HI (57% w/w stabilised with 1.5% H_3PO_3) were purchased of the highest purity available and used as received. N-Methyl-1,4-diazabicyclo[2.2.2]octan-1-ium (MDABCO) iodide was synthesised as described elsewhere[45,46]. 0.5 mol MDABCO iodide and ammonium iodide were dissolved in an aqueous HI solution (20%, stabilised with 0.5% H_3PO_3) at 90 °C. Cooling the pale yellow solution to room temperature resulted in the precipitation of white polycrystalline material. Washing with EtOH and Et_2O and drying in a vacuum gave MDNI as a white crystalline solid in 70% yield. MDNI monocrystals for Raman spectroscopy were grown by first forming a saturated solution of MDNI in DI water at 90 °C, followed by slow cooling down to 60 °C. Over several days large monocrystals of MDNI were formed.

B. MDNI fibre production

Capillary tubes were used as received from Polymicro. The tubes were warmed on a hotplate at 95 °C, then dipped in a solution of 0.2 g MDNI powder that was fully dissolved in 0.16 mL of deionised water that had been filtered through 0.45 µm hydrophilic filter and kept at 95 °C to allow the solution to fill the tube through capillary action. The tubes were then introduced into a homemade 'crystallisation oven' consisting of two metal plates and a spacer that was pre-warmed to 95 °C. The filled capillary was held in the oven for 24 h at 95 °C to ensure that any crystal that might have formed in the setup phase would redissolve, and secondly to start the crystal formation through evaporation at the capillary edge. The fibre was then cooled down slowly at a linear rate of $0.5\,^{\circ}\mathrm{C\,h^{-1}}$.

C. Materials characterisation

Powder X-ray diffraction data of the produced MDNI were acquired on a Bruker D8 Advance diffractometer in coupled theta / two theta regime. Single crystal measurements were taken of the MDNI fibre mounted in a Lindemann tube. The data was collected using an Oxford Cryosystems low-temperature device operated at $T = 100(2)$ K and a Rigaku FRE+ equipped with VHF Varimax confocal mirrors, an AFC12 goniometer, and a HyPix 6000 detector diffractometer. The resulting data was resolved using Rigaku CrysAlis Pro. Raman spectra were collected in the backscattering geometry with 0.5 mW, 532 nm laser excitation focused to a spot size of 1 µm using a Horiba Raman microscope.

D. Linear optical characterisation

The optical transmission losses of the fibres were measured using the standard cut-back technique. The fibre was mounted in a larger host capillary and polished using standard 'dry' fibre polishing methods, i.e., no liquid lubricants were used. A low power continuous wave 1550 nm laser diode was used with an output power of 2 mW. The laser was launched into the core of the fibre using a 0.65 NA anti-reflection coated fused silica objective that was selected to ensure the light was coupled predominantly into the fundamental core mode. The output of the fibre was imaged using an Interlaced CCD IR camera to confirm that transmission occurred only through the semiconductor core, thus providing a good indication of the bulk MDNI material quality. The coupling was optimized using a set of Thorlabs Nanomax stages. The measurements were performed on sections of fibre that were 1 cm in length and each cutback removed approximately 1 mm of the fibre. Modal isolation was undertaken using off-axis launching of light and the light was coupled out of the fibre using a 0.65 NA lens that is greater than the fibre's NA. The captured light was imaged using the interlaced CCD IR camera and coupling into each mode was optimised using the Nanomax stages while observing the imaged output.

E. Nonlinear optical characterisation

The 5 µm core MDNI optical fibre was prepared in the same manner as for the linear optical characterisation measurements. A Spectra Physics Spirit-One femtosecond laser with a wavelength of 1040 nm, a repetition rate of 1 kHz, and a pulse duration of 300 fs was launched into the fundamental mode of the fibre using a 0.65 NA anti-reflection coated fused silica objective and the coupling was optimised using Thorlabs Nanomax stages and viewing on a near-IR CCD camera. The second-harmonic output was imaged on a visible CCD camera with an integration of 10 frames.

V. SUPPLEMENTARY MATERIALS

See the supplementary materials for additional information.

ACKNOWLEDGMENTS

This work was supported by the UK's Engineering and Physical Sciences Research Council (EPSRC) on grant number EP/S031103/1. We thank the EPSRC UK National Crystallography Service at the University of Southampton for the collection of the crystallographic data.

DATA AVAILABILITY STATEMENT

The data that support the findings of this study are available from the corresponding author upon reasonable request.

[1]F. A. Martinsen, B. Smeltzer, M. Nord, T. Hawkins, J. Ballato, and U. Gibson, "Silicon-core glass fibres as microwire radial-junction solar cells," Scientific reports **4**, 1–7 (2014).

[2]R. He, T. D. Day, M. Krishnamurthi, J. R. Sparks, P. J. Sazio, V. Gopalan, and J. V. Badding, "Silicon p-i-n junction fibers," Advanced Materials **25**, 1461–1467 (2013).

[3]R. He, P. J. Sazio, A. C. Peacock, N. Healy, J. R. Sparks, M. Krishnamurthi, V. Gopalan, and J. V. Badding, "Integration of gigahertz-bandwidth semiconductor devices inside microstructured optical fibres," Nature Photonics **6**, 174–179 (2012).

[4]P. Mehta, N. Healy, T. Day, J. Badding, and A. Peacock, "Ultrafast wavelength conversion via cross-phase modulation in hydrogenated amorphous silicon optical fibers," Optics express **20**, 26110–26116 (2012).

[5]T. Sørgård, T. Hawkins, J. Ballato, U. L. Österberg, and U. J. Gibson, "All-optical high-speed modulation of thz transmission through silicon core optical fibers," Optics Express **29**, 3543–3552 (2021).

[6]L. Shen, N. Healy, L. Xu, H. Cheng, T. Day, J. Price, J. Badding, and A. Peacock, "Four-wave mixing and octave-spanning supercontinuum generation in a small core hydrogenated amorphous silicon fiber pumped in the mid-infrared," Optics Letters **39**, 5721–5724 (2014).

[7]A. C. Peacock, J. Campling, A. F. Runge, H. Ren, L. Shen, O. Aktas, P. Horak, N. Healy, U. J. Gibson, and J. Ballato, "Wavelength conversion and supercontinuum generation in silicon optical fibers," IEEE Journal of Selected Topics in Quantum Electronics **24**, 1–9 (2017).

[8]R. Sohanpal, H. Ren, L. Shen, C. Deakin, A. M. Heidt, T. W. Hawkins, J. Ballato, U. J. Gibson, A. C. Peacock, and Z. Liu, "All-fibre heterogeneously-integrated frequency comb generation using silicon core fibre," Nature communications **13**, 1–8 (2022).

[9]S. Song, N. Healy, S. Svendsen, U. Österberg, A. C. Covian, J. Liu, A. Peacock, J. Ballato, F. Laurell, M. Fokine, *et al.*, "Crystalline gasb-core optical fibers with room-temperature photoluminescence," Optical Materials Express **8**, 1435–1440 (2018).

[10]S. Song, K. Lønsethagen, F. Laurell, T. Hawkins, J. Ballato, M. Fokine, and U. J. Gibson, "Laser restructuring and photoluminescence of glass-clad gasb/si-core optical fibres," Nature communications **10**, 1–7 (2019).

[11]J. Zhang, T. Zhang, H. Zhang, Z. Wang, C. Li, Z. Wang, K. Li, X. Huang, M. Chen, Z. Chen, *et al.*, "Single-crystal snse thermoelectric fibers via laser-induced directional crystallization: from 1d fibers to multidimensional fabrics," Advanced Materials **32**, 2002702 (2020).

[12]D. A. Coucheron, M. Fokine, N. Patil, D. W. Breiby, O. T. Buset, N. Healy, A. C. Peacock, T. Hawkins, M. Jones, J. Ballato, *et al.*, "Laser recrystallization and inscription of compositional microstructures in crystalline sige-core fibres," Nature communications **7**, 1–9 (2016).

[13]J. R. Sparks, R. He, N. Healy, M. Krishnamurthi, A. C. Peacock, P. J. Sazio, V. Gopalan, and J. V. Badding, "Zinc selenide optical fibers," Advanced Materials **23**, 1647–1651 (2011).

[14]T. Zaengle, U. J. Gibson, T. W. Hawkins, C. McMillen, B. Ghimire, A. M. Rao, and J. Ballato, "A novel route to fibers with incongruent and volatile crystalline semiconductor cores: Gaas," ACS Photonics **9**, 1058–1064 (2022).

[15]A. Peacock, U. Gibson, and J. Ballato, "Silicon optical fibres–past, present, and future," Advances in Physics: X **1**, 114–127 (2016).

[16]N. Healy, U. Gibson, and A. C. Peacock, "A review of materials engineering in silicon-based optical fibres," Semiconductor Science and Technology **33**, 023001 (2018).

[17]M. G. Coco, S. C. Aro, S. A. McDaniel, A. Hendrickson, J. P. Krug, P. J. Sazio, G. Cook, V. Gopalan, and J. V. Badding, "Continuous wave fe 2+: Znse mid-ir optical fiber lasers," Optics Express **28**, 30263–30274 (2020).

[18]F. Deng, Y. Ren, Z. Wang, S. Xia, Z. Gu, and Y. Wang, "Microfibers Doped with Perovskite Nanocrystals for Ultralow-Loss Waveguides," ACS Applied Nano Materials **2**, 6585–6591 (2019).

[19]Z. Wang, H. He, S. Liu, H. Wang, Q. Zeng, Z. Liu, Q. Xiong, and H. J. Fan, "Air Stable Organic–Inorganic Perovskite Nanocrystals@Polymer Nanofibers and Waveguide Lasing," Small **16**, 2004409 (2020).

[20]W. Wang, M. Zhang, F. Deng, Z. Wang, and Y. Wang, "Hybrids of perovskite nanocrystals and SiO2 microfiber for robust and long-haul transmittable fiber lasers," Applied Physics Letters **119**, 051102 (2021).

[21]N. Kurahashi, V.-C. Nguyen, F. Sasaki, and H. Yanagi, "Whispering gallery mode lasing in lead halide perovskite crystals grown in microcapillary," Applied Physics Letters **113**, 011107 (2018).

[22]Y. Zhou, M. A. Parkes, J. Zhang, Y. Wang, M. Ruddlesden, H. H. Fielding, and L. Su, "Single-crystal organometallic perovskite optical fibers," Science advances **8**, eabq8629 (2022).

[23]R. Zhang, J. Fan, X. Zhang, H. Yu, H. Zhang, Y. Mai, T. Xu, J. Wang, and H. J. Snaith, "Nonlinear optical response of organic–inorganic halide perovskites," Acs Photonics **3**, 371–377 (2016).

[24]M. R. Filip, G. E. Eperon, H. J. Snaith, and F. Giustino, "Steric engineering of metal-halide perovskites with tunable optical band gaps," Nature communications **5**, 1–9 (2014).

[25]F. O. Saouma, D. Y. Park, S. H. Kim, M. S. Jeong, and J. I. Jang, "Multiphoton absorption coefficients of organic–inorganic lead halide perovskites ch3nh3pbx3 (x= cl, br, i) single crystals," Chemistry of Materials **29**, 6876–6882 (2017).

[26]H. Syed, W. Kong, V. Mottamchetty, K. J. Lee, W. Yu, V. R. Soma, J. Yang, and C. Guo, "Giant nonlinear optical response in triple cation halide mixed perovskite films," Advanced Optical Materials **8**, 1901766 (2020).

[27]G. Walters, B. R. Sutherland, S. Hoogland, D. Shi, R. Comin, D. P. Sellan, O. M. Bakr, and E. H. Sargent, "Two-photon absorption in organometallic bromide perovskites," ACS nano **9**, 9340–9346 (2015).

[28]Y.-H. Kim, S. Kim, A. Kakekhani, J. Park, J. Park, Y.-H. Lee, H. Xu, S. Nagane, R. B. Wexler, D.-H. Kim, *et al.*, "Comprehensive defect suppression in perovskite nanocrystals for high-efficiency light-emitting diodes," Nature Photonics **15**, 148–155 (2021).

[29]R. J. Sutton, G. E. Eperon, L. Miranda, E. S. Parrott, B. A. Kamino, J. B. Patel, M. T. Hörantner, M. B. Johnston, A. A. Haghighirad, D. T. Moore, *et al.*, "Bandgap-tunable cesium lead halide perovskites with high thermal stability for efficient solar cells," Advanced Energy Materials **6**, 1502458 (2016).

[30]W. Shen, J. Chen, J. Wu, X. Li, and H. Zeng, "Nonlinear optics in lead halide perovskites: mechanisms and applications," ACS Photonics **8**, 113–

124 (2020).
[31]Z.-K. Tan, R. S. Moghaddam, M. L. Lai, P. Docampo, R. Higler, F. Deschler, M. Price, A. Sadhanala, L. M. Pazos, D. Credgington, *et al.*, "Bright light-emitting diodes based on organometal halide perovskite," Nature nanotechnology **9**, 687–692 (2014).
[32]C. Li, H. Wang, F. Wang, T. Li, M. Xu, H. Wang, Z. Wang, X. Zhan, W. Hu, and L. Shen, "Ultrafast and broadband photodetectors based on a perovskite/organic bulk heterojunction for large-dynamic-range imaging," Light: Science & Applications **9**, 1–8 (2020).
[33]B. R. Sutherland and E. H. Sargent, "Perovskite photonic sources," Nature Photonics **10**, 295–302 (2016).
[34]H.-Y. Ye, Y.-Y. Tang, P.-F. Li, W.-Q. Liao, J.-X. Gao, X.-N. Hua, H. Cai, P.-P. Shi, Y.-M. You, and R.-G. Xiong, "Metal-free three-dimensional perovskite ferroelectrics," Science **361**, 151–155 (2018).
[35]M. G. Ehrenreich, Z. Zeng, S. Burger, M. R. Warren, M. W. Gaultois, J.-C. Tan, and G. Kieslich, "Mechanical properties of the ferroelectric metal-free perovskite [mdabco](nh 4) i 3," Chemical Communications **55**, 3911–3914 (2019).
[36]D. Sirbu, H. C. L. Tsui, N. Alsaif, S. Iglesias-Porras, Y. Zhang, M. Wang, M. Liu, A. C. Peacock, P. Docampo, and N. Healy, "Wide-band-gap metal-free perovskite for third-order nonlinear optics," ACS Photonics **8**, 2450–2458 (2021).
[37]T. W. Kasel, Z. Deng, A. M. Mroz, C. H. Hendon, K. T. Butler, and P. Canepa, "Metal-free perovskites for non linear optical materials," Chemical Science **10**, 8187–8194 (2019).
[38]T. Handa, R. Hashimoto, G. Yumoto, T. Nakamura, A. Wakamiya, and Y. Kanemitsu, "Metal-free ferroelectric halide perovskite exhibits visible photoluminescence correlated with local ferroelectricity," Science advances **8**, eabo1621 (2022).
[39]X. Song, Q. Li, J. Han, C. Ma, Z. Xu, H. Li, P. Wang, Z. Yang, Q. Cui, L. Gao, *et al.*, "Highly luminescent metal-free perovskite single crystal for biocompatible x-ray detector to attain highest sensitivity," Advanced Materials **33**, 2102190 (2021).
[40]N. Gupta, C. McMillen, R. Singh, R. Podila, A. Rao, T. Hawkins, P. Foy, S. Morris, R. Rice, K. Poole, *et al.*, "Annealing of silicon optical fibers," Journal of Applied Physics **110**, 093107 (2011).
[41]D. Marcuse, "Loss analysis of single-mode fiber splices," Bell system technical journal **56**, 703–718 (1977).
[42]T. Ehmke, A. Knebl, S. Reiss, I. R. Fischinger, T. G. Seiler, O. Stachs, and A. Heisterkamp, "Spectral behavior of second harmonic signals from organic and non-organic materials in multiphoton microscopy," AIP advances **5**, 084903 (2015).
[43]Y. Gao, S. Meshkat, A. Johnston, C. Zheng, G. Walters, Q. Feng, X. Wang, M.-J. Sun, A. M. Najarian, D. Xue, *et al.*, "Electro-optic modulation using metal-free perovskites," ACS Applied Materials & Interfaces **13**, 19042–19047 (2021).
[44]X. Wang and Y. Yan, "Molecular engineering of metal-free perovskite mdabco-nh4i3 towards enhanced ferroelectric polarization," arXiv preprint arXiv:2206.11137 (2022).
[45]A. Vasilev, T. Deligeorgiev, N. Gadjev, and K.-H. Drexhage, "Synthesis of novel monomeric and homodimeric cyanine dyes based on oxazolo [4, 5-b] pyridinium and quinolinium end groups for nucleic acid detection," Dyes and pigments **66**, 135–142 (2005).
[46]A. Kurutos, I. Orehovec, D. Saftić, L. Horvat, I. Crnolatac, I. Piantanida, and T. Deligeorgiev, "Cell penetrating, mitochondria targeting multiply charged dabco-cyanine dyes," Dyes and Pigments **158**, 517–525 (2018).